

Submillimetre and far-infrared spectroscopy of monodeuterated amidogen radical (NHD):
improved rest-frequencies for astrophysical observations

LUCA BIZZOCCHI,¹ MATTIA MELOSSO,² BARBARA MICHELA GIULIANO,¹ LUCA DORE,²
FILIPPO TAMASSIA,³ MARIE-ALINE MARTIN-DRUMEL,⁴ OLIVIER PIRALI,^{4,5} LAURENT MARGULÈS,⁶ AND
PAOLA CASELLI¹

¹*Center for Astrochemical Studies, Max-Planck-Institut für extraterrestrische Physik,
Gießenbachstr. 1, 85748 Garching bei München (Germany)*

²*Dipartimento di Chimica “G. Ciamician”, Università di Bologna,
via F. Selmi 2, 40126 Bologna (Italy)*

³*Dipartimento di Chimica Industriale “Toso Montanari”, Università di Bologna,
viale del Risorgimento 4, 40136 Bologna (Italy)*

⁴*Institut des Sciences Moléculaires d’Orsay (ISMO), CNRS, Univ. Paris-Sud, Université Paris-Saclay,
F-91405 Orsay, France*

⁵*SOLEIL Synchrotron, AILES beamline, l’Orme des Merisiers, Saint-Aubin, F-91190 Gif-sur-Yvette, France*

⁶*Université Lille, CNRS, UMR8523 - PhLAM - Physique des Lasers Atomes et Molécules, F-59000 Lille,
France*

(Received June 16, 2020; Revised revision date; Accepted acceptance date;
Published published date)

Submitted to ApJS

ABSTRACT

Observations of ammonia in interstellar environments have revealed high levels of deuteration, and all its D-containing variants, including ND₃, have been detected in cold prestellar cores and around young protostars. The observation of these deuterated isotopologues is very useful to elucidate the chemical and physical processes taking place during the very early stages of star formation, as the abundance of deuterated molecules is highly enhanced in dense and cold gas. Nitrogen hydride radicals are key species lying at the very beginning of the reaction pathway leading to the formation of NH₃ and organic molecules of pre-biotic interest, but relatively little information is known about their D-bearing isotopologues. To date, only ND has been detected in the interstellar gas. To aid the identification of further deuterated nitrogen radicals, we have thoroughly re-investigated the rotational spectrum of NHD employing two different instruments: a frequency-modulation submillimetre spectrometer operating in the THz region and a synchrotron-based Fourier Transform infrared

Corresponding author: Luca Bizzocchi
bizzocchi@mpe.mpg.de

Corresponding author: Mattia Melosso
mattia.melosso2@unibo.it

spectrometer operating in the 50–240 cm^{-1} frequency range. NHD was produced in a plasma of NH_3 and D_2 . A wide range of rotational energy levels has been probed thanks to the observation of high N (up to 15) and high K_a (up to 9) transitions. A global analysis including our new data and those already available in the literature has provided a comprehensive set of very accurate spectroscopic parameters. A highly reliable line catalogue has been generated to assist archival data searches and future astronomical observations of NHD at submillimetre and THz regimes.

Keywords: ISM: molecules – line: identification – molecular data – infrared: ISM – submillimetre: ISM – radio lines: ISM

1. INTRODUCTION

Nitrogen is amongst the most abundant elements in the Universe and is a constituent of essentially all molecules which are important for life as we know it. Nitrogen-bearing species are also ubiquitous in the interstellar medium (ISM) and circumstellar envelopes where about 60 such molecules have been detected to date (McGuire 2018, see also <http://astrochymist.org/> and CDMS*, Endres et al. 2016). The main molecular reservoir of nitrogen in the ISM is believed to be the homonuclear form N_2 . Observation of this molecule, however, is extremely challenging: first, the lack of a permanent dipole moment due its centrosymmetric nature prevents this species from having a rotational signature; second, its vibrational mode is infrared inactive. Consequently, a single interstellar detection of N_2 through its electronic spectrum in the far ultraviolet has been reported to date (Knauth et al. 2004). The study of nitrogen chemistry in space thus mainly relies on observations of other molecules.

Light nitrogen hydrides as imidogen (NH), amidogen (NH_2), and ammonia (NH_3) are involved in the very first steps of the reaction network which leads to the formation of complex species, and are thus of primary importance to constrain the models describing nitrogen chemistry in the ISM. They are formed by a chain of hydrogen abstraction reactions starting from:



and that produce the ions NH_2^+ , NH_3^+ , and NH_4^+ , which are connected to the corresponding neutral hydrides by dissociative recombination reactions. (Le Gal et al. 2014; Dislaire et al. 2012).

The ion–neutral process (1) is endothermic and is thus very sensitive to the H_2 ortho-to-para ratio in the cold ($T < 20$ K) and dense ISM. Also, if H_2 is replaced with its singly deuterated form HD, the endothermicity of (1) is reduced (see, e.g. Cernicharo et al. 2013) thus favouring, in principle, the formation of ND^+ and further D-substituted species (the so called “fractionation”). However, given that the HD/ H_2 ratio keeps about constants to $\sim 10^{-5}$ (Linsky 2007), this route is rather inefficient, and it is likely that reactions of neutral

* Cologne Database for Molecular Spectroscopy, <https://cdms.astro.uni-koeln.de/classic/>

species with H_2D^+ , which abund in the dense and cold environment, could be efficient drivers of D-fractionation (e.g. Sipilä et al. 2019). This process is triggered by the favorable thermochemistry (deuterated isotopologues typically have lower zero-point energy than the corresponding parent species), and if suitable chemical conditions are met (i.e. freeze-out of CO onto dust grains Caselli et al. 1999, 2002), it can be very effective in enhancing the abundances of D-bearing species in cold and dense environments.

Albeit statistically improbable owing to the relatively low cosmic elemental abundance of deuterium ($\text{D}/\text{H} \sim 1.6 \times 10^{-5}$), multiply deuterated variants of ammonia are known to be present in space (see, e.g., Roueff et al. 2005), including the triply substituted ND_3 (Lis et al. 2002; van der Tak et al. 2002) whose estimated abundance ($\text{ND}_3/\text{NH}_3 \sim 10^{-3} - 10^{-4}$) implies an isotopic enhancement of up to 12 orders of magnitude (Ceccarelli et al. 2007).

Interestingly enough, among the ammonia progenitors, only ND has been detected in space so far (Bacmann et al. 2010, 2016) even though significant abundances of NHD and ND_2 are predicted by chemical models (Roueff et al. 2005). To explain such lack of detection, one has to point out that nitrogen hydride radicals are elusive species. Being light molecules, their rotational spectral features are located in the submillimetre (submm) to far-infrared (FIR) ranges, where Earth-based observations face the limitation of the high atmospheric opacity. This spectral window has been widely opened in the last decade by the *Herschel Space Telescope* campaign (Pilbratt et al. 2010), thus triggering an increased interest for the spectroscopic properties of light molecules, hydrides in particular. Nowadays, with ALMA at its full capabilities, wide portions of the submm regime up to ~ 1 THz have become more accessible from the ground, and further perspectives can be foreseen with the improvement of the SOFIA airborne observatory (see, e.g. Yorke et al. 2018), in particular, with the upcoming commissioning of the 4GREAT receiver, which is designed to replicate most of the spectral coverage of the *Herschel*/HIFI instrument. Still, high-frequency observations remain a challenging task and a successful detection of the spectral features of light molecular tracers critically depends on the accuracy of the corresponding rest-frequencies.

From a spectroscopic point of view, the parent species NH_2 has been widely studied in the laboratory over the past 40 years (Davies et al. 1976; Hills & Cook 1982; Charo et al. 1981; Tonooka et al. 1997; Müller et al. 1999; Gendriesch et al. 2001; Martin-Drumel et al. 2014), while much less extensive data sets are available for the other amidogen isotopologues. Driven by the perspectives of the current observational facilities, the symmetric species $^{15}\text{NH}_2$ and ND_2 species have been recently re-investigated at high resolution in the millimetre (mm) and FIR domains (Margulès et al. 2016; Melosso et al. 2017), and the rotational spectrum of the fully substituted $^{15}\text{ND}_2$ variant has been reported for the first time (Melosso et al. 2019). A thorough spectroscopic study is still missing for the asymmetric singly-substituted NHD species, which is likely to be the most abundant deuterated variant of amidogen in the ISM. In the early '80s, the hyperfine structure of a few lines of NHD were observed by Microwave-Optical Double Resonance (MODR) technique (Brown & Steimle 1980; Steimle et al. 1980), whereas the first extensive investigation of its rotational

spectrum was accomplished much later by [Morino & Kawaguchi \(1997\)](#) who employes a Fourier-Transform (FT) FIR spectrometer. Almost simultaneously, [Kobayashi et al. \(1997\)](#) published an analogous study in the mm/submm domain using a microwave absorption spectrometer. In the former case, the spectral resolution did not allow the observation of the hyperfine structure but the spectral coverage ($103\text{--}363\text{ cm}^{-1}$) led to a detailed centrifugal distortion analysis. In the latter case, hyperfine splittings were resolved for many transitions, and several spin-spin and spin-rotation constants were determined for ^{14}N , H, and D.

In this work, we report on: (i) the extension towards the THz regime of the rotational spectrum of NHD with high measurement accuracy, i.e., better than 100 kHz, and (ii) a re-investigation of its FIR spectrum, recorded at higher resolution (0.001 cm^{-1}) using synchrotron radiation at the AILES beamline of the SOLEIL synchrotron. Newly observed and previously recorded data were analysed together in order to produce a unique set of highly accurate spectroscopic constants. The structure of the paper is the following: In § 2, we describe the laboratory measurements; in § 3, we provide an account of the data used in the analysis and give a brief description of the Hamiltonian employed to compute the rotational, fine-structure, and hyperfine energies. We discuss the results in § 4, and draw our conclusions in § 5.

2. EXPERIMENTS

High-resolution pure rotational spectral data of NHD have been collected in the submm region at the Centre for Astrochemical Studies of the Max-Planck-Institut für extraterrestrische Physik in Garching (CAS@MPE) and in the FIR domain at the AILES beamline of the SOLEIL synchrotron in Gif-sur-Yvette.

The measurements in Garching have been carried out using the CASAC (CAS Absorption Cell) spectrometer associated to a discharge absorption cell for the studies of reactive species ([Bizzocchi et al. 2018](#)). A detailed description of the instrument has been given earlier ([Bizzocchi et al. 2017](#)); we report here only a few key details which apply to the present investigation. Several solid-state multiplier/amplifier chains (Virginia Diodes), driven by a radio-frequency synthesizer, have been used as radiation sources. Below 1.1 THz we have employed the WR9.0SGX module, working in the 80–125 GHz interval, associated to a series of active and passive harmonic doublers/triplers in cascade, thus achieving a frequency multiplication factors as high as 9. Measurements above this frequency have been performed with a stand-alone active multiplier system operating in the 1.1–1.2 THz (AMC-680) interval. Accurate frequency and phase stabilisation is achieved by locking the parent centimetre synthesizer to a Rb atomic clock. A closed-cycle He-cooled InSb hot electron bolometer operating at 4 K (QMC) is used as a detector. The measurements have been performed using the frequency modulation (FM) technique to improve the signal-to-noise ratio (S/N). In each frequency range, the FM depth was chosen to approximately match the Doppler half-width of the absorption signals, i.e, 500 kHz at 0.5 THz, and 1300 kHz at 1.2 THz. The carrier signal is modulated by a 33.3 kHz sine-wave and the detector output

is demodulated at twice this frequency using a phase sensitive amplifier ($2f$ detection). In this way, the second derivative of the actual absorption profile is recorded by the computer controlled acquisition system. An additional S/N improvement is achieved by filtering the signal into a RC circuit.

The NHD radical was produced in a glow discharge (70 mA, ~ 1.1 kV) of a 1:2 mixture of NH_3 ($4 \mu\text{bar}$) and D_2 ($8 \mu\text{bar}$) diluted in Ar buffer (total pressure $\sim 25 \mu\text{bar}$), with the cell kept at ~ 180 K by cold vapour/liquid N_2 circulation. Besides preventing cell overheating, the cooling was found to be critical to improve the amidogen production in the plasma. However, below the indicated temperature, NHD signals decreased due to massive ammonia condensation on the cold cell walls. The spectrum was recorded in selected frequency regions from 430 GHz to 1.2 THz. Slow ($0.67\text{--}1.67 \text{ MHz s}^{-1}$) back-and-forth scans around target lines were performed employing a frequency step of $10\text{--}25$ kHz and a time constant $RC = 3$ ms.

The FIR spectrum of NHD has been recorded at the synchrotron facility SOLEIL using a Bruker IFS125HR FTIR spectrometer exploiting the bright synchrotron radiation extracted by the AILES beamline. The spectrum results from the co-addition of 104 scans recorded at the ultimate resolution of the instrument, $R = 0.001 \text{ cm}^{-1}$ in terms of Bruker definition, in the $50\text{--}250 \text{ cm}^{-1}$ range. A $6 \mu\text{m}$ Mylar beamsplitter and a 4.2 K liquid helium cooled bolometer were used. The NHD radical was produced using a post-discharge set-up successfully employed in the past to produce the NH_2 and NH radicals as well as their ^{15}N isotopic variants (Martin-Drumel et al. 2014; Margulès et al. 2016; Bailleux et al. 2012). In this configuration, a radiofrequency discharge cell is connected perpendicularly to the center of a White-type multipass absorption cell. In the present work, a 2.5 m baselength White-type cell allowing 150 m of absorption path length was used (Pirali et al. 2012). The absorption cell was separated from the interferometer by two polypropylene films of $60 \mu\text{m}$ thickness. The spectrometer was pumped down to 10^{-4} mbar by means of a turbomolecular pump, while the flow in the post-discharge experiment was ensured by a booster pump. The NHD radical was produced by a 1000 W radiofrequency discharge (Martin-Drumel et al. 2011) in a $\text{ND}_3 + \text{H}_2$ mixture at partial pressures of 30 and $15 \mu\text{bar}$, respectively. Production of NHD, as well as ND_2 , were found to be more efficient when the gas mixture was injected at one end of the absorption cell while pumping connections were set at the other end of that cell, so that no gas was directly injected through the RF discharge cell. Such configuration enabled a propagation of the plasma into the absorption cell. A discharge-off spectrum was also recorded to quickly identify the lines arising from transient species.

3. OBSERVED SPECTRA AND ANALYSIS

Monodeuterated amidogen is an asymmetric-top rotor belonging to the C_s point group symmetry. Because of the presence of one unpaired electron in a a'' non-bonding orbital, NHD is a radical with a \tilde{X}^2A'' electronic ground state. The electric dipole moment lies in the ab principal symmetry plane with components $\mu_a = 0.67$ D and $\mu_b = 1.69$ D (Brown et al. 1979). The rotational spectrum of NHD is very complex due to the coupling of the

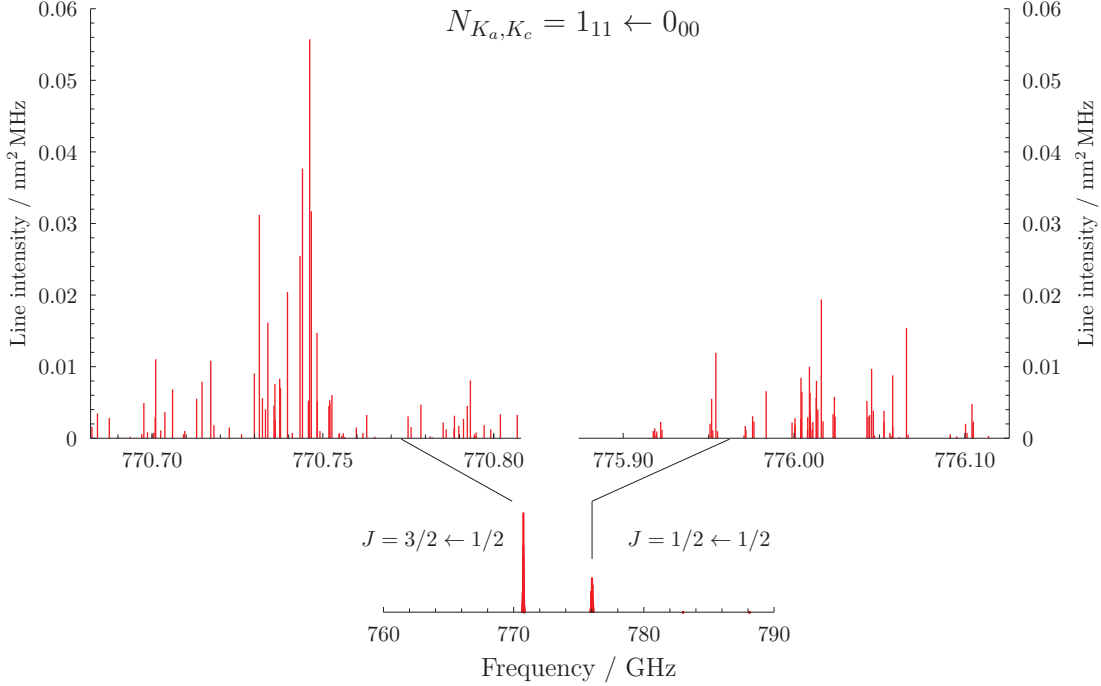


Figure 1. Stick spectrum of the $N_{K_a, K_c} = 1_{11} - 0_{00}$ rotational transition of NHD simulated at 298 K.

molecular rotation with various electronic and nuclear spin angular momenta. The electron spin ($S = 1/2$) couples with the rotational angular momentum and splits each rotational level with $N > 0$ into two fine-structure sublevels having $J = N + 1/2$ and $J = N - 1/2$ quantum numbers. Each of these sublevels is further split by hyperfine interactions due to the nuclear spins of ^{14}N ($I = 1$), H ($I = 1/2$), and D ($I = 1$). The chosen angular momentum coupling scheme can be summarised as:

$$\mathbf{J} = \mathbf{N} + \mathbf{S} \quad (2a)$$

$$\mathbf{F}_1 = \mathbf{J} + \mathbf{I}_N \quad (2b)$$

$$\mathbf{F}_2 = \mathbf{F}_1 + \mathbf{I}_H \quad (2c)$$

$$\mathbf{F} = \mathbf{F}_2 + \mathbf{I}_D \quad (2d)$$

where \mathbf{N} and \mathbf{S} are the rotational and electron spin angular momenta, whereas \mathbf{I}_X ($X = \text{N, D, H}$) represents the various nuclear spin angular momenta. In Eqs. (2), the nuclear spins are ordered according to the approximate magnitude of their hyperfine coupling.

The effective Hamiltonian can be expressed as a sum of several energy contributions as in the following (Morino & Kawaguchi 1997; Kobayashi et al. 1997):

$$\tilde{H}_{\text{eff}} = \tilde{H}_{\text{rot}} + \tilde{H}_{\text{sr}} + \tilde{H}_{\text{hfs}}. \quad (3)$$

Here, \tilde{H}_{rot} is the Watson A-reduced Hamiltonian in its I' representation (Watson 1977), which includes the rotational energy and the centrifugal distortion (up to the J^{12} terms in the present analysis). The fine-structure Hamiltonian \tilde{H}_{sr} contains the electron spin-rotation

terms (ϵ tensor) and their centrifugal dependencies. The \tilde{H}_{hfs} term is the hyperfine-structure Hamiltonian which includes electronic spin-nuclear spin interactions (a_F , \mathbf{T}) and nuclear spin-nuclear spin coupling (\mathbf{C}) for all the three nuclei, and the electric quadrupole coupling contributions (χ) for the ^{14}N and D nuclei, having $I \geq 1$. The spectral computation was performed using the SPFIT/SPCAT suite of programs (Pickett 1991) which implements all the matrix elements of the Hamiltonian (3) in the coupling scheme (2).

Unlike the symmetric species NH_2 and ND_2 , for which a π rotation around the b principal axis exchanges two identical particles, there are no spin statistics in the case of NHD. Consequently, all fine and hyperfine sublevels, up to a maximum of 36, are allowed for each N_{K_a, K_c} rotational level. The electric dipole selection rules (Gordy & Cook 1984) on this sublevels manifold produce very complex hyperfine patterns for each rotational transition due to the additional fine/hyperfine selection rules $\Delta J = 0, \pm 1$, $\Delta F_1 = 0, \pm 1$, $\Delta F_2 = 0, \pm 1$, and $\Delta F = 0, \pm 1$. The most intense components have $\Delta J = \Delta F_1 = \Delta F_2 = \Delta F = \Delta N$. An example of the complexity is given in Figure 1, which illustrates the above described interactions for the fundamental b -type transition $N_{K_a, K_c} = 1_{11} - 0_{00}$. Each line of the fine-structure doublet, separated by some GHz, is then split in a multitude of hyperfine components, roughly gathered in loose triplets, due to the dominant effect of electron spin-nuclear spin coupling due to the ^{14}N nucleus.

Table 1. List of NHD rotational transitions with HFS recorded in the submillimetre region.

line	type ^a	unsplit freq. (MHz)	no. of FS lines	no. of HFS lines
1 _{1,0} - 1 _{0,1}	${}^b Q_{+1,-1}$	432580.3	4	44
2 _{0,2} - 1 _{1,1}	${}^b R_{-1,+1}$	456235.5	2	5
2 _{1,1} - 2 _{0,2}	${}^b Q_{+1,-1}$	515448.6	2	19
3 _{1,2} - 3 _{0,3}	${}^b Q_{+1,-1}$	656654.9	2	30
1 _{1,1} - 0 _{0,0}	${}^b R_{+1,+1}$	772506.7	2	15
4 _{1,3} - 4 _{0,4}	${}^b Q_{+1,-1}$	869336.3	2	7
3 _{0,3} - 2 _{1,2}	${}^b R_{-1,+1}$	902924.7	2	12
3 _{2,1} - 3 _{1,2}	${}^b Q_{+1,-1}$	1020828.9	2	5
6 _{2,4} - 6 _{1,5}	${}^b Q_{+1,-1}$	1062344.6	2	6
2 _{1,2} - 1 _{0,1}	${}^b R_{+1,+1}$	1112159.2	2	4
3 _{1,3} - 2 _{1,2}	${}^a R_{0,+1}$	1122794.6	1	1
5 _{1,4} - 5 _{0,5}	${}^b Q_{+1,-1}$	1157071.0	1	6
3 _{0,3} - 2 _{0,2}	${}^a R_{0,+1}$	1199330.9	2	6

^a The symbol ${}^x M_{\delta K_a, \delta K_c}$ is used to label in a compact form the transition type for an asymmetric rotor: x indicates the dipole moment component involved, $M = P, Q, R$ is the symbol for the transitions with $\Delta N = -1, 0, +1$, respectively, and δK_a and δK_c refer to the (signed) change in the K_a and K_c pseudo-angular quantum numbers (Gordy & Cook 1984).

3.1. Submillimetre spectrum

The spectral recordings performed with the CASAC spectrometer covered the frequency interval from 430 GHz to 1200 GHz, exploring the region above 520 GHz for the first time. Since NHD is a very light molecule, the rotational transitions are quite isolated in the spectrum and separated by several tens of GHz. The transitions recorded in this frequency domain are summarized in Table 1, which also reports the hypothetically unsplit frequency of the rotational lines and the number of assigned hyperfine components.

Under our experimental conditions, isolated NHD absorption lines have a full width at half maximum (FWHM) of 1.5–3.0 MHz due to the sizable Doppler broadening characteristic of this spectral range (e.g., $\Delta\nu_G^{\text{FWHM}} \sim 1.5$ MHz at 700 GHz for NHD at 150 K). However, due to the complexity of the hyperfine structure, overlap of numerous components is common and blends of lines, resolved to different extents, are typically observed. To facilitate the retrieval of the corresponding central line frequencies, we have modeled the recorded absorption profiles using the proFFiT line analysis code (Dore 2003) adopting a FM Voigt profile function and considering the full complex representation of the Fourier-transformed dipole correlation function. When necessary, the background contribution has also been accounted for using a third-order polynomial expansion. In most cases, this approach typically allowed for a satisfactory fit of the recorded spectral profiles, with some minor discrepancies due to the occasional presence of noise features or weak interfering lines. An example is presented in Figure 2, which shows the recordings of the $N_{K_a, K_c} = 4_{1,3} \leftarrow 4_{0,4}, J = 9/2 \leftarrow 9/2$ fine-structure component of NHD: **eighteen** hyperfine components are blended in six resolvable lines illustrating the predominance of the N coupling ($I_N = 1$, three main groups), followed by the H coupling ($I_H = 1/2$, closely separated doublets). The modeled profile has been obtained by fixing the Doppler FWHM at 1.834 MHz (computed at 150 K) and adjusting the line positions and the Lorentzian FWHM (collisional broadening), $\Delta\nu_G^{\text{FWHM}} = 1.42(15)$ MHz, assumed equal for all the components. The described procedure allowed us to obtain line positions with an associate error in the 30–100 kHz interval, depending on the S/N of the spectrum and on the overall goodness of the line profile fit.

Whenever possible, a single hyperfine transition has been assigned to a given resolved feature detected in the rotational spectrum. Measurements corresponding to tight line blends have been instead assigned to the subset of components which sum up to make the dominant intensity contribution. In these cases the intensity-averaged frequency is compared with the experimental one in the least-squares fit. Loose blends of unresolved components, resulting in very broad or distorted line profiles, have not been used in the analysis.

3.2. Far infrared spectrum

The recorded FIR spectrum was calibrated using residual water lines whose accurate frequencies have been reported in the literature (Matsushima et al. 1995); the resulting accuracy on line frequency is estimated to be of 0.0002 cm^{-1} . Deuterium scrambling in

$$N_{K_a, K_c} = 4_{1,3} \leftarrow 4_{0,4}, J = \frac{9}{2} \leftarrow \frac{9}{2}$$

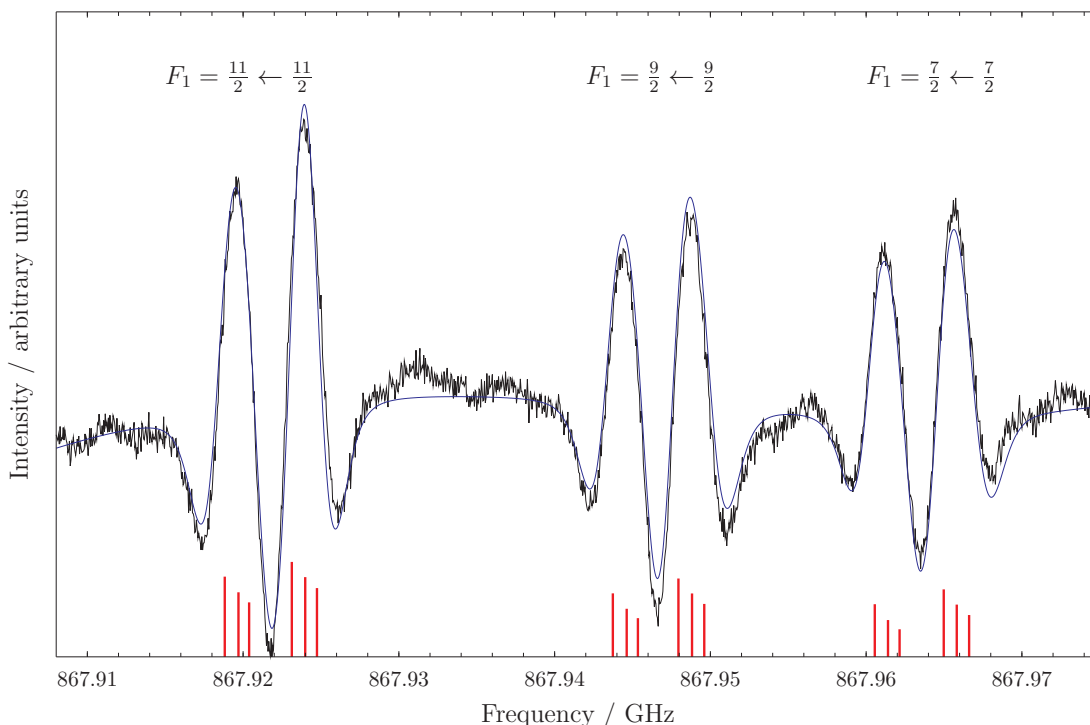


Figure 2. Recording (black trace) of the $N_{K_a, K_c} = 4_{1,3} \leftarrow 4_{0,4}, J = \frac{9}{2} \leftarrow \frac{9}{2}$ fine-structure transitions showing six resolvable components. Integration time: 390 s; $RC = 3$ ms; scanning rate: 1.3 MHz/s; modulation depth: 850 kHz. The blue trace plots the modeled spectrum computed with proFFiT using a modulated Voigt profile (see text). The red sticks indicates the position and relative intensity of the eighteen hyperfine components. Note that the F_2 and F quantum numbers are not shown in the plot.

the $\text{ND}_3 + \text{H}_2$ discharge mixture appears very efficient as strong transitions of NHD are observed. About 10 of the strongest lines are saturated and have been excluded from the analysis. As a point of comparison, under the same experimental conditions, in pure ND_3 or NH_3 , similarly strong signals of ND_2 and NH_2 , respectively, are observed, while in the present spectrum only relatively weak signals of ND_2 (10 % absolute absorption at best) and no NH_2 are observed.

As previously observed in similar studies on the NH_2 radical and its isotopologues (Martin-Drumel et al. 2014; Margulès et al. 2016), the hyperfine splitting due to the nitrogen atom is partially or fully resolved for several b -type transitions on the FIR spectrum, as illustrated in Fig. 3. Because the natural width of the transitions is smaller than the experimental resolution in this spectral region, many lines exhibit a cardinal sine profile at their base (arising from the boxcar apodization). While this effect can be canceled by applying an apodization to the interferogram before Fourier transform, the resulting width broadening prevented from the resolution of the nitrogen hyperfine structure on most transitions; consequently such apodization was not applied.

In total, 512 transitions have been assigned to 447 experimental frequencies in the range $54\text{--}236\text{ cm}^{-1}$, 141 a -type and 371 b -type transitions with $N'_{\text{max}} = 15$ (for $K'_a = 0 - 2$) and

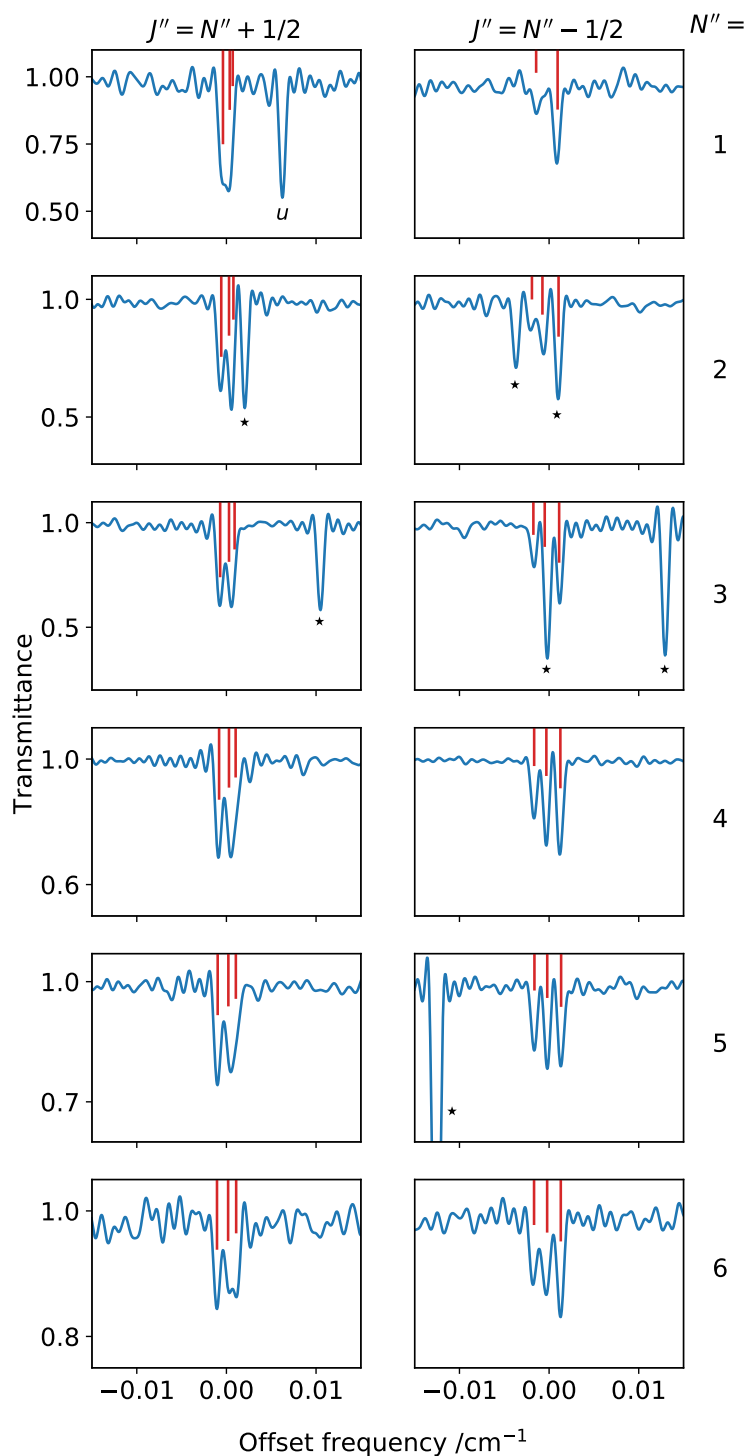


Figure 3. Observation on the FIR spectrum of the hyperfine structure due to the nuclear spin of the N atom in NHD for the b -type ${}^rR(1)$ branch with $K_a'' + K_c'' - N'' = 0$. Frequencies are reported as the offset frequencies from the predicted transition when no hyperfine structure is taken into account and span the 68–188 cm^{-1} range (see the supplementary material for the numerical values). Predicted frequency of each component (neglecting the H and D hyperfine splittings) is indicated by red sticks (intensity in arbitrary units). Transitions labelled with “★” symbol are still present with the discharge off and most likely arise from ND_3 ; the line labelled with a “ u ” remains unassigned.

$K'_{a_{\max}} = 7$ (for $N' = 7$). Among these transitions, 107 transitions (80 different frequencies, mostly b -type) with $K'_a = 0 - 3$ exhibit partially or fully resolved nitrogen hyperfine structure. The uncertainty on line frequency is doubled for lines that appear broadened by unresolved hyperfine structure or asymmetric splitting.

4. RESULTS

The experimental frequencies were fitted to the Hamiltonian of Eq. (3) in a least-square procedure, in which the weight of each datum was proportional to the inverse square of its error. The data set includes previously measured (Morino & Kawaguchi 1997; Kobayashi et al. 1997) and newly observed mm-, submm-wave, and FIR transitions. The data from Morino & Kawaguchi (1997) were given uncertainties of $7.5 \times 10^{-4} \text{ cm}^{-1}$, i.e., an order of magnitude smaller than their resolution of 0.0075 cm^{-1} , while the errors reported in Kobayashi et al. (1997) were retained. A total of 58 spectroscopic parameters could be determined from the analysis of more than 1000 distinct frequencies. Their values are reported in Table 2–3 and compared with the results of former studies.

All the observed transition frequencies could be fitted within their experimental uncertainty: the weighted deviation of the fit is close to one ($\sigma = 0.96$) and the rms error is 52 kHz for transitions in the mm-/submm-wave region and $4.1 \times 10^{-4} \text{ cm}^{-1}$ for those in the FIR ($1.9 \times 10^{-4} \text{ cm}^{-1}$, for the transitions recorded in this work). While the studies of Morino & Kawaguchi (1997) and Kobayashi et al. (1997), published almost simultaneously, provided two different sets of constants relying on different data sets, our global analysis comprises all those transitions, in addition to a larger set of submm-wave and FIR data. To this respect, a more comprehensive set of spectroscopic constants is produced in this work. Overall, the rotational, centrifugal distortion, and fine-interaction constants of Table 2 are now refined, and their values agree well with those reported previously by the cited authors. Still, some sporadic discrepancies are present, e.g., the Φ_{NK} constant determined by Kobayashi et al. (1997) is two times larger than ours and has opposite sign. The hyperfine-interaction parameters are almost identical to those of Kobayashi et al. (1997), because the magnitude of the hyperfine coupling effect decreases with the increase of the rotational quantum numbers involved in the transitions. We have determined 23 hyperfine constants, three more than in Kobayashi et al. (1997), namely: $\chi_{bb} - \chi_{cc}$ for the nucleus D, $\Delta^J T_{aa}$, and C_{cc} for the nucleus H. The magnitude of these parameters is small and they are determined with a precision of 30% at best. Still their inclusion in the fit allowed to reduce the σ by 10%, thus they have been retained in the final analysis.

While the semi-rigid rotor Hamiltonian used in this work allows to nicely reproduce the experimental data at their experimental accuracy, owing to the use of high order centrifugal distortion terms, it is possible, however, that the present analysis reaches its limits. Indeed, 7 additional transitions involving high $N + K_a$ values have been assigned with relative confidence on the FIR spectrum but could not be reproduced in the fit. As for NH_2 (Martin-Drumel et al. 2014), a dedicated model taking into account the anomalous centrifugal distortion of this very light radical may be better suited to reproduce these data.

Table 2. Rotational and fine-structure spectroscopic parameters determined for NHD.

Constants		Present work	Kobayashi et al. (1997)	Morino & Kawaguchi (1997)
A	/MHz	602874.1082(64)	602873.269(18)	602879.3(24)
B	/MHz	243153.818(15)	243150.415(29)	243147.6(9)
C	/MHz	169872.513(15)	169875.877(26)	169871.5(9)
Centrifugal distortion				
Δ_N	/MHz	9.29361(23)	9.2833(9)	9.239(9)
Δ_{NK}	/MHz	31.2187(11)	30.303(13)	31.226(45)
Δ_K	/MHz	250.2294(21)	250.825(10)	250.90(21)
δ_N	/MHz	3.07038(10)	3.04088(12)	3.0672(30)
δ_K	/MHz	48.7864(81)	46.854(14)	47.502(66)
Φ_N	/kHz	1.0098(24)		0.785(42)
Φ_{NK}	/MHz	0.04883(14)	-0.0901(11)	0.04569(60)
Φ_{KN}	/MHz	-0.17115(50)		-0.1638(21)
Φ_K	/MHz	0.79326(48)	0.59213(25)	0.8223(87)
ϕ_N	/kHz	0.4888(12)		0.475(18)
ϕ_{NK}	/MHz	0.023248(49)		0.02099(42)
ϕ_K	/MHz	0.2588(11)		0.1256(19)
L_{NNK}	/kHz	-2.373(14)		
L_{KKN}	/kHz	0.0437(32)		0.0615(84)
L_K	/kHz	-3.91(29)		-3.20(17)
l_K	/kHz	0.307(22)		0.0210(48)
P_K	/Hz	8.43(29)		17.6(16)
p_K	/Hz	-1.40(16)		
O_K	/Hz	-0.0196(18)		-0.0591(57)
Fine interaction				
ϵ_{aa}	/MHz	-7043.123(16)	-7043.180(27)	-7041.0(12)
ϵ_{bb}	/MHz	-1149.383(17)	-1149.38(9)	-1150.96(45)
ϵ_{cc}	/MHz	7.809(17)	7.82(8)	8.7(11)
$(\epsilon_{ab} + \epsilon_{ba})/2$	/MHz	1088.64(60)	1093.9(11)	1056(7)
Δ_N^S	/MHz	0.12026(78)	0.1187(20)	0.140(9)
Δ_{KN+NK}^S	/MHz	0.2401(87)		
Δ_{NK}^S	/MHz	1.77(35)	0.234(13)	
Δ_K^S	/MHz	16.2441(91)	16.245(12)	16.16(21)
δ_N^S	/MHz	0.06300(30)	0.0640(7)	0.075(8)
δ_K^S	/MHz	0.9553(83)	0.96(4)	1.20(11)
Φ_K^S	/MHz	-0.06755(59)	-0.0634(7)	-0.0570(45)
L_K^S	/kHz	0.2270(96)		0.135(30)
Number of FIR lines		649		
Number of MW lines		353		
σ_{FIR}	/cm ⁻¹	4.2×10^{-4}		
σ_{MW}	/kHz	51.8		
σ_w		0.963		
$N'_{\text{max}}, K'_{a,\text{max}}$		15,9		

NOTE: Numbers in parenthesis are one standard deviation in units of the last quoted digit.

Considering the small number of transitions involved, however, no attempt was made in

Table 3. Hyperfine spectroscopic parameters (MHz) determined for NHD.

Constant	Atom	This work	Kobayashi et al. (1997)
a_F	(N)	28.1077(71)	28.124(10)
$\Delta^K a_F$	(N)	0.0	-0.0157(12)
T_{aa}	(N)	-43.3319(77)	-43.329(8)
T_{bb}	(N)	-44.2125(97)	-44.218(11)
T_{ab}	(N)	0.550	0.550
χ_{aa}	(N)	-0.288(13)	-0.297(14)
$(\chi_{bb} - \chi_{cc})$	(N)	-6.738(28)	-6.725(32)
χ_{ab}	(N)	1.370	1.370
C_{aa}	(N)	0.3486(33)	0.3505(37)
C_{bb}	(N)	0.0738(29)	0.0742(37)
χ_{aa}	(D)	0.167(15)	0.143(40)
$(\chi_{bb} - \chi_{cc})$	(D)	0.100(44)	
a_F	(D)	-10.230(10)	-10.229(13)
T_{aa}	(D)	8.0530(91)	8.052(10)
T_{bb}	(D)	-7.251(13)	-7.251(14)
T_{ab}	(D)	6.1(14)	6.7(14)
C_{aa}	(D)	0.0482(34)	0.0491(36)
a_F	(H)	-67.128(11)	-67.116(13)
T_{aa}	(H)	-23.305(31)	-23.254(24)
T_{bb}	(H)	28.460(23)	28.434(22)
T_{ab}	(H)	-47.9(19)	-48.7(20)
$\Delta^K T_{aa}$	(H)	-0.122(16)	-0.0621(51)
$\Delta^J T_{aa}$	(H)	0.0192(69)	
C_{aa}	(H)	0.0844(75)	0.1152(64)
C_{bb}	(H)	0.0864(50)	0.1042(60)
C_{cc}	(H)	-0.0157(48)	

NOTE: Numbers in parenthesis are one standard deviation in units of the last quoted digit.
Parameters without reported deviation were kept fixed in the fit.

this direction in the present study and these transitions are reported in the supplementary material.

5. CONCLUSIONS

The rotational spectrum of NHD has thoroughly been re-investigated from the submm region to the FIR. A frequency-modulation spectrometer and a synchrotron-based FT spectrometer were used to perform the measurements. Numerous *a*-type and *b*-type transitions have been recorded with high accuracy, i.e., 30–100 kHz for lines up to 1.2 THz and $2 \times 10^{-4} \text{ cm}^{-1}$ in the 50–240 cm^{-1} frequency range. Also, the astronomically important $N_{K_a, K_c} = 1_{11} - 0_{00}$ fundamental *b*-type transition has been observed in the laboratory for the first time and its fine and hyperfine components have been accurately measured around 770 GHz ($J = 3/2 - 1/2$) and 776 GHz ($J = 1/2 - 1/2$).

The newly obtained set of spectroscopic parameters (Tables 2 and 3) allow to generate a very reliable set of rest-frequencies for NHD in the submm and FIR spectral domains. Considering all rotational transitions originating from levels at energy E/h lower than 300 K, their corresponding rest-frequencies have a 1σ uncertainty of less than 10 m s^{-1} (in radial equivalent velocity) up to 3 THz. Two different CDMS-like catalogues based on the present spectral calculations, with hyperfine structure fully resolved or ^{14}N coupling only, are provided as supplementary material. This comprehensive laboratory study opens new perspectives for the first identification of NHD in space, which would enable to make a step towards a more complete understanding of ammonia formation in the ISM. The highly precise rest-frequencies provided here enable to carry out focused searches in the observation data of Herschel Legacy Archive (<http://archives.esac.esa.int/hsa/whsa/>) and also provides a basis for new observations in the presently accessible spectral windows employing facilities like ALMA or the upcoming 4GREAT instrument on board SOFIA.

ACKNOWLEDGMENTS

This study was supported by Bologna University (RFO funds) and by MIUR (Project PRIN 2015: STARS in the CAOS, Grant Number 2015F59J3R). The work at SOLEIL has been performed under the proposal 20110017 and was supported by the Programme National “Physique et Chimie du Milieu Interstellaire” (PCMI) of CNRS/INSU with INC/INP co-funded by CEA and CNES.

SUPPLEMENTARY MATERIAL

The catalogue `nhd_full_hfs.cat` lists all the hyperfine components originated by ^{14}N , D, and H nuclear couplings and extends up to 2 THz ($150 \mu\text{m}$). The catalogue `nhd_n_hfs.cat` contains a computation of the hyperfine spectrum due to the ^{14}N coupling only and extends into the FIR domain ($8 \text{ THz} \sim 38 \mu\text{m}$). The file `center_frequencies.dat` reports the reference frequencies used in Figure 3. The file `discarded_transitions.dat` contains those transitions which could not be reproduced in the fit and were excluded from the analysis. The machine-readable table `measured_transitions.mrt` lists all measured transition frequencies and fit residuals.

REFERENCES

- Bacmann, A., Caux, E., Hily-Blant, P., et al. 2010, *A&A*, 521, L42
- Bacmann, A., Daniel, F., Caselli, P., et al. 2016, *A&A*, 587, 26
- Bailleux, S., Martin-Drumel, M. A., Margulès, L., et al. 2012, *A&A*, 538, A135
- Bizzocchi, L., Lattanzi, V., Laas, J., et al. 2017, *A&A*, 602, A34
- Bizzocchi, L., Melosso, M., Dore, L., et al. 2018, *ApJL*, 863, 3
- Brown, J. M., Chalkley, S. W., & Wayne, F. D. 1979, *Mol. Phys.*, 38, 1521
- Brown, J. M. & Steimle, T. C. 1980, *ApJL*, 236, 101
- Caselli, P., Walmsley, C. M., Tafalla, M., Dore, L., & Myers, P. C. 1999, *ApJ*, 523, L165
- Caselli, P., Walmsley, C. M., Zucconi, A., et al. 2002, *ApJ*, 565, 344
- Ceccarelli, C., Caselli, P., Herbst, E., Tielens, A. G. G. M., & Caux, E. 2007, in *Protostars and Planets V*, ed. B. Reipurth, D. Jewitt, & K. Keil, 47
- Cernicharo, J., Tercero, B., Fuente, A., et al. 2013, *ApJL*, 771, L10
- Charo, A., Herbst, E., De Lucia, F. C., & Sastry, K. V. L. N. 1981, *ApJL*, 94, 244
- Davies, P. B., Russell, D. K., Thrush, B. A., & Radford, H. E. 1976, *Chem. Phys. Lett.*, 42, 35
- Dislaire, V., Hily-Blant, P., Faure, A., et al. 2012, *A&A*, 537, A20
- Dore, L. 2003, *J. Mol. Spectrosc.*, 221, 93
- Endres, C. P., Schlemmer, S., Schilke, P., Stutzki, J., & Müller, H. S. P. 2016, *J. Mol. Spectrosc.*, 327, 95
- Gendriesch, R., Lewen, F., Winnewisser, G., & Müller, H. S. P. 2001, *J. Mol. Struct.*, 599, 293
- Gordy, W. & Cook, R. L. 1984, *Microwave molecular spectra* (Wiley, New York)
- Hills, G. W. & Cook, J. M. 1982, *J. Mol. Spectrosc.*, 94, 456
- Knauth, D. C., Andersson, B. G., McCandliss, S. R., & Warren Moos, H. 2004, *Nature*, 429, 636
- Kobayashi, K., Ozeki, H., Saito, S., Tonooka, M., & Yamamoto, S. 1997, *J. Chem. Phys.*, 107, 9289
- Le Gal, R., Hily-Blant, P., Faure, A., et al. 2014, *A&A*, 562, A83
- Linsky, J. L. 2007, *Space Sci. Rev.*, 130, 367
- Lis, D. C., Roueff, E., Gerin, M., et al. 2002, *ApJ*, 571, L55
- Margulès, L., Martin-Drumel, M. A., Pirali, O., et al. 2016, *A&A*, 591, A110
- Martin-Drumel, M. A., Pirali, O., Balcon, D., et al. 2011, *Rev. Sci. Instrum.*, 82, 113106
- Martin-Drumel, M. A., Pirali, O., & Vervloet, M. 2014, *J. Phys. Chem. A*, 118, 1331
- Matsushima, F., Odashima, H., Iwasaki, T., Tsunekawa, S., & Takagi, K. 1995, *J. Mol. Struct.*, 352-353, 371
- McGuire, B. A. 2018, *ApJS*, 239, 17
- Melosso, M., Conversazioni, B., Degli Esposti, C., et al. 2019, *J. Quant. Spectrosc. Radiat. Transfer*, 222, 186
- Melosso, M., Degli Esposti, C., & Dore, L. 2017, *ApJS*, 233, 15
- Morino, I. & Kawaguchi, K. 1997, *J. Mol. Spectrosc.*, 182, 428
- Müller, H. S. P., Klein, H., Belov, S. P., et al. 1999, *J. Mol. Spectrosc.*, 195, 177
- Pickett, H. M. 1991, *J. Mol. Spectrosc.*, 148, 371
- Pilbratt, G. L., Riedinger, J. R., Passvogel, T., et al. 2010, *A&A*, 518, L1
- Pirali, O., Boudon, V., Oomens, J., & Vervloet, M. 2012, *J. Chem. Phys.*, 136, 024310
- Roueff, E., Lis, D. C., van der Tak, F. F. S., Gerin, M., & Goldsmith, P. F. 2005, *A&A*, 438, 585
- Sipilä, O., Caselli, P., & Harju, J. 2019, *A&A*, 631, A63
- Steimle, T. C., Curl, R. F., J., & Brown, J. M. 1980, *J. Chem. Phys.*, 73, 2552
- Tonooka, M., Yamamoto, S., Kobayashi, K., & Saito, S. 1997, *J. Chem. Phys.*, 106, 2563
- van der Tak, F. F. S., Schilke, P., Müller, H. S. P., et al. 2002, *A&A*, 388, L53
- Watson, J. K. G. 1977, in *Vibrational Spectra and Structure*, ed. J. Durig, Vol. 6 (Elsevier, Amsterdam), 1–89

Yorke, H. W., Young, E. T., & Becklin, E. E.
2018, in Society of Photo-Optical
Instrumentation Engineers (SPIE)
Conference Series, Vol. 10700,
Proceedings of the SPIE, 107000E